Polymer Chemistry

PAPER

View Article Online
View Journal | View Issue

Cite this: *Polym. Chem.*, 2016, **7**, 6231

POSS semitelechelic $A\beta_{17-19}$ peptide initiated helical polypeptides and their structural diversity in aqueous medium†

Ujjal Haldar, Abhishek Pan, Ishita Mukherjee and Priyadarsi De*

Biomolecule promoted helical polypeptides and their structural diversity towards external/internal stimuli is an interesting research area to the material science community. In this report, we have synthesized sequence registered peptide–polypeptide conjugates *via* ring opening polymerization (ROP) of γ-benzyl-L-glutamate *N*-carboxyanhydride (BLG-NCA) employing two amine terminated peptide initiators, namely H-Phe-Val-Leu-POSS (POSS: polyhedral oligomeric silsesquioxane; Leu: leucine; Val: valine; Phe: phenylalanine) and H-Phe-Val-Leu-OMe. Main chain POSS semitelechelic or POSS free tripeptide containing poly(γ-benzyl-L-glutamate) (PBLG) homopolymers adopted α-helical conformation in both solution and the solid state, because of intramolecular hydrogen bonding and π–π aromatic interactions between side chain phenyl groups. POSS/OMe tripeptide conjugated PBLG segments self-assembled into hierarchical ordered helical entangled nanofibres, revealed by tapping mode atomic force microscopy (AFM) and field emission-scanning electron microscopy (FE-SEM). Expulsion of side chain benzyl groups (crucial for π–π aromatic interaction and stabilizing groups for the secondary structure scaffold) produced pH-sensitive amphiphilic anionic homopolymers, which exhibited diverse self-assembled nanoparticles in aqueous medium at pH 8.0. Interestingly, a morphological switch from sphere to square shaped micelles could be achieved simply by adjusting the net fraction of POSS moiety and/or the length of the benzyl deprotected segment.

Received 11th August 2016,
Accepted 15th September 2016

DOI: 10.1039/c6py01399f

www.rsc.org/polymers

Introduction

Polypeptides are an interesting class of naturally occurring bioactive materials which have received significant attention as biomaterials owing to their close relationship with proteins.[1,2] Conjugation of polypeptides with proteins/sequence registered peptides has opened up a new platform for a wide range of functional biomaterials such as drug and gene delivery carriers, ligand–protein interactions, tissue-engineering scaffolds, biomedical imaging agents, antimicrobial agents, *etc.*,[3,4] because of their flexibility in terms of functionality and their molecular recognition properties.[5,6] Based on amino acid composition, polypeptides can adopt α-helix, β-sheet, random coil or turn structures in solution as well as in the bulk state.[7] Among the various synthetic polypeptides, poly(γ-benzyl-L-glutamate) (PBLG) is a useful chiral building block for the creation of both α-helix, β-sheet secondary structures *via* intra-/inter-molecular hydrogen bonding interactions depending upon the degree of polymerization (DP) of the PBLG segment.[8,9] In addition, such polypeptides can self-assemble into well-defined macromolecular architectures in selected solvents.[10]

Polypeptides containing a single amino acid residue can be prepared *via* ring opening polymerization (ROP) of *N*-carboxyanhydrides (NCAs) using amine terminated initiators.[11] Among the various organic/inorganic initiators, initiation of α-amino acid containing NCA monomers using bioactive precursors (such as peptide, lipid, *etc.*) is always more accepted and demanding in the field of applied biomaterials, because it leads to the generation of new kinds of hybrid biomaterials.[12] In addition, conjugation of suitable bioactive moieties with the synthetic polypeptide improves biocompatibility, bioreactivity as well as significantly impacting the self-assembling phenomenon of biomolecule–polypeptide conjugates in selected solvent systems.[13] Indeed, a few efforts have been reported in the literature for synthesizing polypeptides using bioactive molecules as initiators. Marsden *et al.* reported a series of amphiphilic polypeptide-*b*-designed peptides in which the hydrophobic block is PBLG and the hydrophilic

Polymer Research Centre, Department of Chemical Sciences, Indian Institute of Science Education and Research Kolkata, Mohanpur - 741246, Nadia, West Bengal, India. E-mail: p_de@iiserkol.ac.in

†Electronic supplementary information (ESI) available: Detailed synthesis and characterization of H-FVL-OMe and H-FVL-POSS tripeptides, additional scheme and figures as noted in the main text. See DOI: 10.1039/c6py01399f

block is a coiled-coil forming peptide (denoted E). The coiled-coil forming peptide was synthesized on the solid phase, followed by the ROP of γ-benzyl-L-glutamate *N*-carboxyanhydride (BLG-NCA), initiated from the N-terminal amine of the peptide E on the solid support.[14] Recently, comb-polypeptides of repeated peptide sequences were synthesized *via* ROP of peptide appended NCA monomers without aid of any post-polymerization modification.[15] Although peptide–polymer[16,17] and protein–polymer[18,19] conjugates are studied significantly in the literature, conjugates of peptide–polypeptide are less explored, though both the segments are biocompatible and could be crucial for the development of novel biologically relevant systems. Thus, we became inspired to make peptide–polypeptide conjugates comprising of sequence registered peptides and polypeptides in a controlled fashion. To achieve this goal, we have adopted the short peptide motif, Leu-Val-Phe (LVF), from the central hydrophobic cluster of the amyloid β-peptide, $A\beta_{1-42}$, which is responsible for fibril formation in Alzheimer's disease and such LVF derived polymers inhibited fibril formation.[20,21] Also, acetylated derivatives of LVF can act as potent HIV protease inhibitors[22] and showed increased activity against cathepsin D and pepsin.[23]

Polyhedral oligomeric silsesquioxane (POSS)-PBLG copolymers were synthesized through the ROP of BLG-NCA using aminopropyl isobutyl-POSS as an initiator.[24] POSS derivatives belong to organic/inorganic hybrid family,[25] and incorporation of the POSS moiety at the chain ends of PBLG allowed intramolecular hydrogen bonding between the POSS and PBLG units to enhance the α-helical conformation of PBLG in the solid state and prevented aggregation in solution. Lin and Kuo reported linear POSS-*b*-PBLG copolymers by coupling azide terminated POSS with alkyne terminated PBLG homopolymer *via* click chemistry.[26] The POSS-*b*-PBLG systems displayed greater conformational stability as a result of intramolecular hydrogen bonding between the POSS moiety and the PBLG segment, and superior thermal properties compared to pure PBLG. Recently, the same group synthesized linear polypeptide-*graft*-POSS copolymers, where POSS was hanging in the side chains of poly(γ-propargyl-L-glutamate) (PPLG) through click chemistry.[8] In all these cases, the advent of POSS unit either in the side/main chain could stabilize the α-helical secondary structure even at low DP, by improving the side/main chain mobility through its sterically crowded rigid end, and also provided additional hydrogen bonding through the siloxane core (Si–O–Si) with main chain PBLG segments.[27] We were interested combining the POSS tethered amyloidogenic short peptide (LVF) motif with PBLG segments to fabricate a wide variety of hierarchical nanostructures. Therefore, in this present work we have employed POSS semitelechelic $A\beta_{17-19}$ peptide initiator to initiate polymerization of BLG-NCA *via* grafting from the ROP technique. The effect of the POSS moiety on the self-assembly of PBLG was studied in detail. Furthermore, removal of the side chain benzyl groups from the POSS/OMe tripeptide-PBLG conjugates produced pH-sensitive amphiphilic anionic homopolymers, which exhibited diverse self-assembled nanoparticles in aqueous medium.

Experimental section

Materials

γ-Benzyl-L-glutamate (BLG, 99%), Boc-L-phenylalanine (Boc-Phe-OH, 99%), L-valine methyl ester hydrochloride (OMe-Val-NH_3·HCl, 99%) and L-leucine methyl ester hydrochloride (OMe-Leu-NH_3·HCl, 99%) were purchased from Sisco Research Laboratories (SRL) Pvt. Ltd, India and used without further purification. Aminoisobutyl polyhedral oligomeric silsesquioxane (POSS-NH_2) was obtained from Hybrid Plastics, MS, USA. Dicyclohexylcarbodiimide (DCC, 99%) and anhydrous *N*,*N*-dimethylformamide (DMF, 99.9%) were obtained from Sigma Aldrich and used as received. Triphosgene (Spectrochem, India), 1-hydroxybenzotriazole hydrate (HOBt hydrate, Spectrochem), trifluoroacetic acid (TFA, 99.5%, Merck, India), hydrobromic acid/acetic acid (HBr/AcOH, 33 wt%, Spectrochem), sodium bicarbonate ($NaHCO_3$, Merck) and calcium hydride (CaH_2, Spectrochem) were used without any further purification. Tetrahydrofuran (THF, Merck) was dried over CaH_2 for 24 h and distilled from sodium and benzophenone under N_2 environment prior to use. The NMR solvents such as $CDCl_3$ (99.8% D), DMSO-d_6 (99.8% D) and D_2O (99.8% D) were bought from Cambridge Isotope Laboratories, Inc., USA. General solvents such as hexanes (mixture of isomers), acetone, methanol, ethyl acetate, toluene, dichloromethane (DCM), *etc*. and butyl amine (butyl-NH_2, used as an initiator, Merck) were purified by simple distillation.[28]

Instrumentation and analysis

The ^1H, ^{13}C and ^{29}Si NMR spectroscopic measurements were performed at 25 °C using a 500 MHz Bruker Avance^{III} NMR spectrometer with tetramethylsilane (TMS) as an internal standard. Positive mode electrospray ionization mass spectrometry (ESI-MS) was done on a Q-Tof Micro YA263 high resolution mass spectrometer from Waters Corporation. FT-IR spectra were recorded on KBr pellets using a Perkin-Elmer Spectrum 100 FT-IR spectrometer. The sample films used in this study were sufficiently transparent.[8] Since the polymers contain a significant number of amide groups and are hygroscopic in nature, pure N_2 gas was purged in the spectrometer's optical box to keep the polymer film dry. The number average molecular weights (M_ns) and molecular weight distributions (dispersity, $Đ$) of synthesized polymers were determined using a gel permeation chromatography (GPC) instrument in DMF at 30 °C with a flow rate of 1.0 mL min^{-1} with respect to poly (methyl methacrylate) (PMMA) standards. The system consisted of a Waters Model 515 HPLC pump, Waters Model 2414 refractive index (RI) detector, one PolarGel-M guard column and two 300 × 7.5 mm PolarGel-M columns from Agilent Technologies. A Rigaku Smart Lab powder diffractometer having Cu-Kα radiation (λ = 1.54059 Å) with parallel beam optics attachment was engaged for recording powder X-ray diffraction (PXRD) spectra. Solid powder samples were scanned from 2 to 35° (2θ) with a step interval of 0.2°. The instrument was operated at 45 kV voltage and 200 mA current and calibrated with a standard silicon sample. Circular

dichroism (CD) spectroscopic measurements were performed in a JASCO J-815 CD spectrometer in HPLC grade solvents at room temperature (400 μL quartz cuvette cell, 1.0 mm path-length). Average hydrodynamic diameter (D_h) of the aggregated amphiphilic polymers and zeta potential (ξ) values were determined, respectively, by dynamic light scattering (DLS) and eletrophoretic light scattering (ELS), using a Zetasizer Nano ZS (Malvern Instrument Ltd, Malvern, UK) equipped with a He–Ne laser beam at 658 nm with scattering angle of 173°. Polymer solutions were filtered through a 0.45 μm syringe filter prior to measurement. All the measurements were carried out in aqueous environment at pH 8.0 and average D_h and ξ values were calculated from three replicate measurements and are reported as mean diameter ± standard deviation. Atomic force microscopy (AFM) imaging was recorded in an NT-MDT NTEGRA prima scanning probe microscope operated in semi-contact mode. For field emission-scanning electron microscopy (FE-SEM) study, an aliquot of sample solution (0.1 or 0.01 mg mL^{-1} in THF and H_2O) was drop-casted on a small piece of silicon-wafer and dried completely at room temperature, followed by high vacuum drying. Finally, the specimen was coated with gold–palladium (20 : 80) alloy and images were recorded using a Carl Zeiss-Sigma instrument.

Syntheses of amine terminated initiators

Two free amine terminated sequence defined tripeptide initiators H-Phe-Val-Leu-OMe (H-FVL-OMe) and H-Phe-Val-Leu-POSS (H-FVL-POSS) were synthesized *via* conventional solution phase methodology by using a racemisation free fragment condensation strategy.[29] The details of syntheses procedure (Scheme S1†) and characterization of the peptides are described in the ESI (Fig. S1–S9†).

Synthesis of BLG-NCA monomer

The BLG-NCA monomer was synthesized following a literature procedure[30] with a slight modification. In detail, BLG (10.0 g, 0.042 mol) and triphosgene (4.20 g, 0.014 mol) were suspended in 150 mL of dry THF in a 250 mL double necked round bottom (RB) flask connected with a reflux condenser and N_2 bubbler. The mixture was continuously stirred at 50 °C until the reaction mixture became clear. Then, the reaction was continued for 5–6 h. Finally, the clear solution was concentrated by a rotary evaporator. Note: the temperature of the water bath on the rotary evaporator was kept below 30 °C to minimize the possible side reactions due to unavoidable moisture. After removing the supernatant, the reaction mixture was re-dissolved in 100 mL ethyl acetate. Exactly equal volume of hexanes was added into it to induce crystallization of the NCA monomer. Then, it was kept at −10 °C overnight and the crystals were collected as a white solid powder by suction filtration under N_2 environment. Finally the solid residue was dried under high vacuum condition and stored in a glove box. Yield: 65%. ^{1}H NMR (Fig. S10,† $CDCl_3$, δ, ppm): 7.41–7.32 (m, 5H, Ar*H*), 6.76 (s, 1H, N*H*), 5.13 (s, 2H, Ar–CH_2), 4.41 (m, 1H, H_2C–C*H*–NH), 2.28–2.14 (m, 2H, H_2C–CH–NH). FT-IR (Fig. S11,† cm^{-1}): 3600–3100, 1867, 1844, 1781, 1706, 1257, 1202, 928, 743.

Synthesis of PBLG homopolymers *via* ROP

In a glove box, BLG-NCA (0.20 g, 0.76 mmol), H-FVL-OMe (9.91 mg, 25.3 μmol), 2.0 mL anhydrous DMF and a magnetic spin bar were taken in a 20 mL septum sealed polymerization vial. The mixture was stirred for 72 h at room temperature. Finally, the polymerization was terminated by precipitating into cold methanol. The resulting polymer was collected after repeated reprecipitation (×3) of the polymer solution in acetone from methanol and dried under high vacuum for 12 h at 30 °C. A similar procedure was followed for the synthesis of PBLG using H-FVL-POSS and butyl-NH_2 as initiators. During the polymerization reactions, we restricted monomer conversions below 75% to avoid side reactions.

Deprotection of benzyl groups from PBLG homopolymers

The deprotection of benzyl groups was conducted under strong acid treatment as described elsewhere.[31] Typically, PBLG (**1a** in Table 1, 0.01 g) was dissolved in 1.0 mL THF, followed by addition of 0.5 mL HBr/AcOH (33 wt%) and 0.5 mL TFA. The reaction was continued for 12 h at room temperature. In the next step, the solvent was removed under reduced

Table 1 Characterization of PBLG homopolymers obtained from the polymerization of BLG-NCA in DMF at room temperature in the presence of amine terminated OMe/POSS tripeptide and butyl-NH_2 initiators

Sample	[BLG-NCA]/[I][a]	Initiator (I)	DP_n[b]	Conv.[c] (%)	$M_{n,theo}$[d] (g mol^{-1})	$M_{n,GPC}$ ($Đ$)[e] (g mol^{-1})	$M_{n,NMR}$[f] (g mol^{-1})
1a	20/1	H-FVL-OMe	16	72	4200	4500 (1.18)	4600
1b	30/1	H-FVL-OMe	26	69	5800	7300 (1.20)	7200
1c	60/1	H-FVL-OMe	45	65	10 600	12 400 (1.21)	12 200
2a	20/1	H-FVL-POSS	15	68	4800	5300 (1.20)	5200
2b	30/1	H-FVL-POSS	24	62	6100	7800 (1.22)	7500
2c	60/1	H-FVL-POSS	42	60	10 700	12 900 (1.25)	12 300
3a	20/1	Butyl-NH_2	17	75	4000	3400 (1.15)	4600

[a] Stoichiometric ratio of [BLG-NCA]/[initiator (I)]. [b] Determined by NMR analysis. [c] Conversion (Conv.) was determined by gravimetric analysis. [d] $M_{n,theo}$ values were determined by using equation: $M_{n,theo}$ = ($MW_{initiator}$ + ($MW_{BLG\text{-}NCA}$ × Conv. × [BLG-NCA]/[I])), where $MW_{initiator}$, $MW_{BLG\text{-}NCA}$, [BLG-NCA] and [I] are the molecular weight (MW) of initiator, MW of BLG-NCA, initial concentrations of monomer and initiator, respectively. [e] Measured by GPC in DMF. [f] Calculated from ^{1}H NMR analysis.

pressure. The obtained solid was re-dissolved in THF, and the solution was dialyzed against de-ionized (DI) water for 48 h by using a dialysis bag (spectra/por^R dialysis membrane, molecular weight cut-off (MWCO): 2 kDa). During the dialysis, DI water was changed after every 2–8 h for a total of six times. Finally, water was evaporated under reduced pressure using a rotary evaporator and the polymer was dried in a vacuum oven for 48 h at 40 °C.

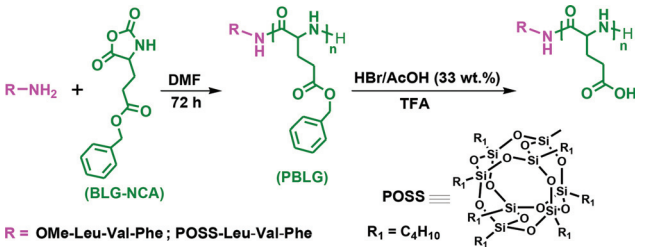

Scheme 1 Synthesis of PBLG using H-FVL-OMe/POSS initiators and deprotection of side-chain benzyl groups from PBLG.

Results and discussion

Syntheses and characterization of peptide initiators

Due to the extreme sensitivity of NCA monomers towards various external/internal physical parameters,[32] it was of prime importance to prepare pure H-FVL-OMe and H-FVL-POSS initiators. These two initiators were characterized by NMR, FT-IR and ESI-MS spectroscopy. ^{1}H NMR spectra of purified H-FVL-OMe (Fig. S1†) and H-FVL-POSS (Fig. S3†) show broad resonance signals at 7.81 and 7.92 ppm, respectively, due to the free amine groups. The peak at 3.62 ppm in Fig. S1† corresponds to –OCH_3 protons in H-FVL-OMe. The signals at 0.56 and 0.92 ppm (Fig. S3†) are due to the methylene (Si–CH_2–) and methyl protons (Si–CH–CH(CH_3)$_2$) of the POSS moiety in H-FVL-POSS, where the POSS segment is covalently connected with one edge of the tripeptide through the C-terminus end. The remainder of the proton signals exhibited by H-FVL-OMe and H-FVL-POSS are assigned carefully to their respective spectra. The ^{13}C NMR spectrum of H-FVL-OMe displays two amide carbonyl signals at 175.4 and 171.7 ppm, along with one ester carbonyl signal at 171.1 ppm (Fig. S2†). However, H-FVL-POSS shows exclusively three amide carbonyl signals at 171.2, 170.5 and 169.8 ppm (Fig. S4†). Fig. S5† depicts silicon resonance signals for the H-FVL-POSS at δ = −67.6 and −67.8 ppm,[33] thus successful covalent attachment of the POSS moiety with the peptide chain end is confirmed. The FT-IR spectrum of H-FVL-OMe (Fig. S6†) and H-FVL-POSS (Fig. S7†) shows informative sharp frequency bands at the region of 1645–1635 and 1556–1535 cm^{-1} due to amide I and II, respectively. In addition, sharp absorption signals appeared at 1746 (Fig. S6†) and 1112 cm^{-1} (Fig. S7†) due to the carbonyl group of the ester functionality of H-FVL-OMe and the Si–O–Si stretching frequency of the POSS moiety. The ESI-mass spectra of H-FVL-OMe (Fig. S8†) and H-FVL-POSS (Fig. S9†) show molecular ion peaks at 392.44 *m*/*z* (molecular weight (MW) of (H-FVL-OMe + H)$^+$) and 1235.10 *m*/*z* (MW of (H-FVL-POSS + H)$^+$), respectively, which matched nicely with the theoretical molecular masses. These observations clearly indicate successful synthesis and high purity of H-FVL-OMe and H-FVL-POSS.

Synthesis of PBLG homopolymers *via* ROP using amine terminated peptide initiators

After successful synthesis of pure H-FVL-OMe and H-FVL-POSS, we have applied them as initiators (I) during the ROP of BLG-NCA at room temperature (Scheme 1). To obtain different molecular weights of the PBLG segment, polymerization reactions were carried out at [BLG-NCA]/[H-FVL-OMe or H-FVL-POSS] ratios between 20 and 60. In addition, one control experiment was carried out to prepare linear PBLG at [BLG-NCA]/[butyl-NH$_2$] = 20 to understand the specific role of both POSS/OMe terminated tripeptide moieties on various physicochemical behaviors of the PBLG segment, such as secondary conformation, self-assembly, *etc*. Polymerization conditions and results are summarized in Table 1. The number average molecular weights ($M_{n,GPC}$) of PBLG polymers were determined by GPC measurements. The molecular weight and $Đ$ values of both the series range from 3100 to 9700 g mol^{-1} and 1.2 to 1.3, respectively (Table 1). On the basis of stoichiometry and monomer conversion (Conv.) of as synthesized homopolymers, we are able to calculate the theoretical number average molecular weight ($M_{n,theo}$) by using the equation: $M_{n,theo}$ = (MW$_{initiator}$ + (MW$_{BLG-NCA}$ × Conv. × [BLG-NCA]/[I])), where MW$_{initiator}$, MW$_{BLG-NCA}$, [BLG-NCA] and [I] are the molecular weight (MW) of initiator, MW of BLG-NCA, initial concentrations of monomer and initiator, respectively. Table 1 shows that the $M_{n,theo}$ values does not fully agree with the corresponding $M_{n,GPC}$ values, plausibly due to the different hydrodynamic volume of OMe/POSS tripeptide end capped PBLG homopolymers with respect to the PMMA standards, which we have employed to construct the conventional calibration curve for $M_{n,GPC}$ measurement.[34]

The chemical structures of POSS/OMe end capped tripeptide-PBLG conjugates were primarily characterized by ^{1}H NMR spectroscopy. Fig. 1A shows informative resonance signals from **1a** at δ (ppm) = 8.53–8.16 (s, 1H, –N*H*–), 7.43–7.01 (s, 5H,

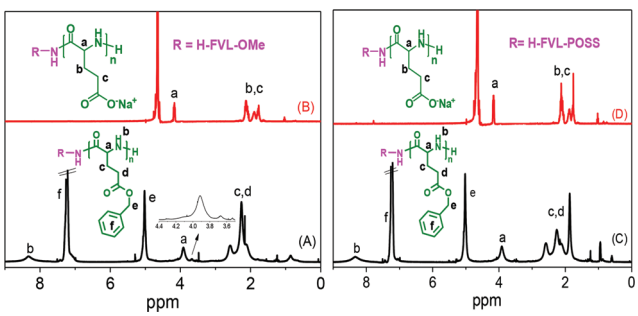

Fig. 1 ^{1}H NMR spectra of (A) **1a** in CDCl$_3$, (B) **d1a** in D$_2$O, (C) **2a** in CDCl$_3$ and (D) **d2a** in D$_2$O.

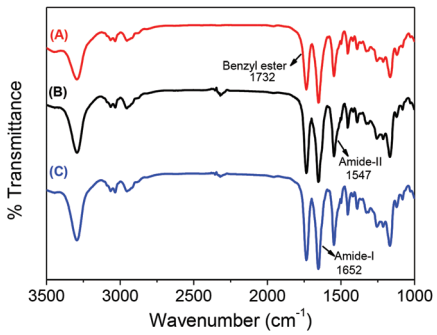

Fig. 2 Solid-state FT-IR spectra of (A) **1a**, (B) **2a** and (C) **3a**.

–Ar*H*), 5.19–4.91 (s, 2H, –Ar–C*H*$_2$–), 4.09–3.78 (t, 1H, –C*H*$_2$CH$_2$C*H*–) and 2.78–1.88 (m, 4H, –C*H*$_2$C*H*$_2$CH$_2$–) along with some low resolved peaks at 3.68–3.66 and 0.91–0.86 ppm corresponding to oxymethyl (–OC*H*$_3$) chain end and methyl (–C*H*$_3$) protons of peptide initiator, respectively. Other proton signals from the initiating moiety were not identified due to their overlapping with the PBLG protons and their low content. Similar ^{1}H NMR spectra were obtained for **2a** (Fig. 1C) and **3a** (Fig. S12†), which were prepared, respectively, by using H-FVL-POSS and butyl-NH$_2$ initiators. Fig. 1C showed resonance signals at 0.57–0.55 and 0.91–0.88 ppm due to the –Si–C*H*$_2$– and –Si–CH–CH(C*H*$_3$)$_2$ protons from the POSS moiety, respectively. Also, the butyl-NH$_2$ initiated polymer **3a** gave an extra peak at 0.92–0.87 ppm for the chain-end methyl protons. Distinct resonance signals from the initiating moiety (at the chain end) and main chain PBLG unit allowed us to calculate the number average molecular weight ($M_{n,NMR}$) from ^{1}H NMR study by using the following formula: $M_{n,NMR}$ = (DP$_{n,BLG\text{-}NCA}$ × MW of BLG-NCA + MW of H-FVL-OMe/H-FVL-POSS/butyl-NH$_2$); where DP$_{n,BLG\text{-}NCA}$ is the degree of polymerization. The DP$_{n,BLG\text{-}NCA}$ of **1a–1c**, **2a–2c** and **3a** were calculated by comparing the intensity of the resonance signals from benzyl protons (2H, C*H*$_2$–Ar) of the PBLG segment with oxymethylene protons (3H, –OC*H*$_3$) of H-FVL-OMe (**1a–1c** series), methylene protons (16H, –Si–C*H*$_2$–) of POSS moiety (**2a–2c** series) and methyl protons (3H, C*H*$_3$–CH$_2$–) of butyl initiator (**3a**), respectively. The $M_{n,NMR}$ values are reported in Table 1, which matched nicely with the $M_{n,GPC}$ values. In addition, the ^{29}Si NMR spectrum of **2a** displayed two peaks from the POSS unit, resonating at δ = −67.6 and −67.8 ppm (Fig. S13†), which clearly showed the presence of the POSS moiety appending with the main chain of the PBLG segment. From the FT-IR spectra of PBLG (Fig. 2), it was not possible to identify amide groups from the initiating moiety (and the Si–O–Si starching frequency in the case of POSS containing PBLG), because of their low content with respect to the amide groups from the PBLG unit. Nevertheless, the above results confirmed successful synthesis of PBLG with POSS/OMe-LVF chain ends.

Secondary conformation of polypeptide segments

To characterize the secondary structure of the designed polypeptides, we have performed FT-IR measurements in both solid and solution state. Fig. 2A shows the partial solid-state FT-IR spectra of **1a**, **2a** and **3a**, where curves look similar. Peaks at 1732 and 1452 cm^{-1} are observed due to the carbonyl group of the ester functionality and phenyl moiety of the side chain PBLG residue, respectively. Absorption bands at 1652 and 1547 cm^{-1} arise from the main chain PBLG homopolymers, which are signatory for amide-I and II, respectively. These two bands are characteristic for α-helical secondary structure of protein/peptide molecules.[9] The secondary conformations of PBLG homopolymers are tremendously dependent on the DP of PBLG units.[35] The FT-IR spectrum of low DP (≤ 10) PBLG showed the amide-I band at 1655–1652 cm^{-1} for α-helix, 1630–1627 cm^{-1} for β-sheet (parallel or antiparallel) and 1695–1692 cm^{-1} for random coil or turn population.[8] Since in our cases the DP of PBLG units are much higher than 10, all the synthesized PBLG homopolymers show exclusively α-helical conformation. In solution phase, we found similar absorption patterns with characteristic helical absorption bands (Fig. S14†). Interestingly, chain end tripeptide segments did not disturb PBLG chains to attain helical conformation governed by the side chain PBLG residues. The possible arrangements of the POSS/OMe tripeptide-PBLG homopolymers are pictorially represented in Fig. S15.†

To further understand the effect of DP on the secondary conformations of PBLG homopolymers, PXRD patterns of **1a**, **1b**, **1c** (Fig. 3) and **2a**, **2b**, **2c** (Fig. S16†) were recorded at 25 °C. In every case, we found one sharp diffraction peak at 2θ = 6.30° due to the α-helical structures.[26] No peaks were found at 2θ = 2.0–5.0°, which would represent the distance between the backbones in the antiparallel β-pleated sheet structures.[26] The three reflections at a ratio 1 : 3$^{1/2}$: 4$^{1/2}$ are associated with (10), (11) and (20) reflections of a 2D-hexagonal arrangement of cylinders, which is basically composed of 18/5 α-helices with a cylinder distance of 1.19.[8,36] Polymer **3a** also shows similar diffraction peaks as depicted in Fig. S17.† The broad peak centered at about 2θ = 20° is originated mainly from the amorphous hollow of PBLG units. All the synthesized peptides had DP ≥ 15, which led to stabilize the α-helical secondary structures with much better packing arrangements. Although the positions of the diffraction pattern are quite similar in all sets of polymers, interestingly the intensity of the diffraction peaks

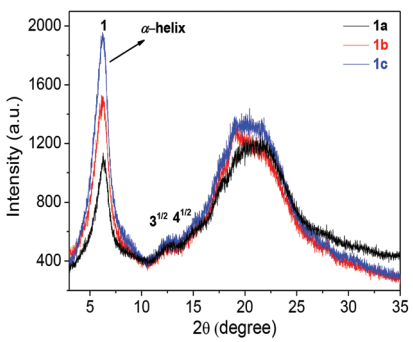

Fig. 3 PXRD spectra of **1a**, **1b** and **1c**.

attains higher value with increasing the DP of the PBLG homopolymer. We believe that longer the chain length of PBLG, the higher is the number of amide bonds which help to stabilize the α-helical secondary structure efficiently *via* intramolecular hydrogen bonding interactions. Another important finding is that the α-helical secondary structure was not disturbed by the bulkier POSS/OMe tripeptide end. Tripeptide chain ends may assist to attain such ordered conformation in the solid state by introducing additional hydrogen bonding motifs.

The secondary conformation of chiral PBLG homopolymers was further studied by CD measurements using dilute polymer solutions (0.2 mg mL^{-1}) in THF, a helicogenic solvent preferred for α-helical secondary structure.[37] It is well known that the PBLG homopolymer can adopt α-helical secondary conformation where pendant phenyl groups extend out of the main chain axis.[38] In this context, π–π aromatic interaction between phenyl groups stabilizes higher order secondary structures. Fig. 4 shows CD spectra of tripeptide initiators and various homopolymers initiated by H-LVF-POSS/OMe. The H-FVL-OMe displays one positive signal at 224 nm and one negative signal at 234 nm, whereas the H-FVL-POSS exhibits one broad signal in the region 222–226 nm. The packing arrangements of both the initiators are entirely different from each other and did not match with any other secondary conformation of protein molecules. Attachment of the POSS moiety to the C-terminus end of the LVF peptide has changed the conformation due to its bulkier sterically organic vertex group. Interestingly, these initiator derived PBLG homopolymers and **3a** (Fig. S18†) exhibited a strong Cotton effect with minima at 222 nm in the CD diagram, a signature for the α-helical secondary conformation of peptides.[39] Polypeptides having α-helical secondary conformations generally show double minima at 222 and 209 nm in the CD spectrum due to the n–π* and parallel-polarized π–π* excitonic transitions, respectively.[40] In our case, we found only one negative minimum at 222 nm, probably due to the strong absorbance of THF at short wavelength range (UV cut off range of THF: 212 nm).[41] Another interesting observation is that the intensity of the negative peak increased with the increasing DP of PBLG. With the increasing DP, the extent of intramolecular hydrogen bonding among the main chain amide linkages and side chain π–π interaction of pendant phenyl groups increases. Although **1a**, **1b**, **1c** and **2a**, **2b**, **2c** are only partially soluble in acetonitrile (turbid solutions after sonication), we obtained two minima at 209 and 222 nm in the CD spectra due to the π–π* and n–π* transitions, thus once again confirming the α-helix secondary conformation of **1a–1c** and **2a–2c** (Fig. S19†).

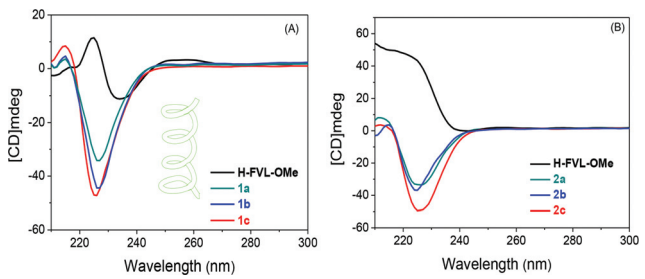

Fig. 4 CD spectra of (A) H-FVL-OMe, **1a**, **1b**, **1c**, and (B) H-FVL-POSS, **2a**, **2b**, **2c** in THF at 20 °C.

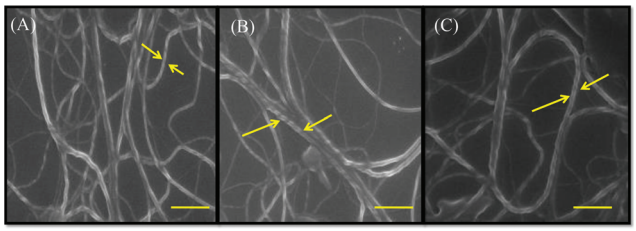

Fig. 5 FE-SEM images of (A) **1c**, (B) **2c** and (C) **3a**. Each scale bar indicates 200 nm. Sample concentration: 0.01 mg mL^{-1}.

Next, self-assembly driven ordered helical nanofibre formation at microscopic level[42] was studied by FE-SEM. Since in our previous experiments we found that extent of helicity is higher at higher DP, we choose **1c** and **2c** for FE-SEM analysis because of their highest DP in the corresponding series. Fig. 5 shows that the **1c**, **2c** and **3a** polypeptides adopted interconnected helical nanofibre structures with an average diameter of ~35 ± 4 nm. This kind of helical turn was predominantly formed because of the side chain phenyl groups in the PBLG, which have the potential to form π–π aromatic interactions. In addition, the side chain PBLG units are chiral in nature and the side-chain spacer is suitable for attaining a helical turn.[43] It is important to note that the concentration of the sample solution is a vital parameter to get a clear insight into the helical entangled nanofibres. The sample film prepared from low concentration polymer solution showed relatively more ordered helical nanofibres having lower average diameter (~35 ± 4 nm) (Fig. 5) in FE-SEM compared to the diameter (~75 ± 10 nm) (Fig. S20†) of the film that was prepared from relatively more concentrated polymer solution. Similar kinds of entangled helical nanofibres from **1c** and **2c** were found by trapping mode AFM microscopic study, shown in Fig. S21.† Thus, POSS/OMe-LVF-PBLG polymers adopted α-helical secondary structure in both bulk and solution state, where the POSS/OMe tripeptide chain end did not affect the secondary conformation of the PBLG.

Deprotection of benzyl groups and self-assembling behaviour

Next, we hydrolyzed benzyl ester groups from the side chains of PBLG to understand the role of benzyl groups (responsible for effective π–π aromatic interaction) in nucleating the structure and to elucidate the effect of the POSS/OMe-tripeptide segment on the solution phase morphology of the polypeptide. Hydrolysis of benzyl ester groups from the side chains of PBLG was accomplished using 33 wt% HBr in glacial AcOH and TFA in THF at room temperature (Scheme 1). Deprotection of benzyl ester groups produced –COOH groups in the side chain, which can be protonated/deprotonated by adjusting the pH of the medium. At basic pH, the resulting polymer is fully soluble in aqueous medium due to the rapid transformation

of –COOH to anionic –COO^-. Deprotected polymers are denoted by adding letter "d" before the sample name. For example, **1a** after deprotection gave **d1a**. Fig. 1 shows the ^{1}H NMR spectra of **d1a** and **d2a** in D_2O at pH 8.0, where resonance signals due to phenyl and benzyl protons respectively at 7.43–7.01 and 5.19–4.91 ppm in the PBLG segment vanished after deprotection reaction. This deprotection phenomenon was further confirmed by FT-IR analysis (Fig. S22†), where stretching frequencies of the carbonyl group of the benzyl ester functionality and phenyl group centered at 1732 and 1452 cm^{-1} completely disappeared after the deprotection reaction and one new peak appeared at 1736 cm^{-1} due to the carbonyl group of the carboxylic acid functionality. Also, the hydroxyl (–OH) stretching frequency (3400–3200 cm^{-1}) was now observed in the same spectra, further indicating deprotection of benzyl groups (data not shown here). The ^{29}Si NMR spectrum of **d2a** (Fig. S23†) displays two silicon resonance signals from the POSS moiety at −67.6 and −67.8 ppm, so showing no decomposition or side reactions of the POSS moiety at the chain end during the deprotection of the benzyl ester groups by such a strong acid treatment. The deprotected polymers are expected to show negative (anionic) surface charges due to the deprotonation of the side chain carboxylic acid groups at basic pH.

This was confirmed by measuring the zeta potential (ξ) values by DLS analysis of aqueous solutions (0.5 mg mL^{-1} at pH 8.0). The net negative ξ values of **d1a**, **d1b**, **d1c**, **d2a**, **d2b** and **d2c** were found to be −24 ± 2, −29 ± 3, −32 ± 4, −22 ± 2, −26 ± 2 and −31 ± 4 mV, respectively. The ξ values increase from **d1a** to **d1b** to **d1c** and **d2a** to **d2b** to **d2c** due to the increasing carboxylate anion content in the side chain of the poly(L-glutamate).

The CD spectra of deprotected polymers were recorded in water at pH 8.0 (Fig. 6). In all cases, the deprotected polymers displayed a negative signal at around 209 nm and a positive signal at 220 nm, corresponding to a random-coil configuration.[44] This occurred owing to the electrostatic repulsion among carboxylate anions in the side chain of the polypeptide backbone. In both the **d1a–d1c** and **d2a–d2c** series, the intensity of the negative minima concomitantly increased with increasing the content of carboxylic anion ends, due to the higher extent of electrostatic repulsion among the side chain carboxylate anion ends.[45] Similarly, **d3a** also shows a random-coil configuration in the CD spectrum, shown in Fig. S24.† Clearly, deprotection of benzyl groups from the PBLG side chains transformed the polymer conformation from α-helical to random-coil.[45]

Amphiphilic polymers can adopt various kinds of morphologies in both solution as well as in the bulk state, such as spherical, worm-like, spindle, cylinders, toroidal, *etc*. depending on the number of hydrophobic/hydrophilic residues, chemical composition and molecular architecture.[45,46] The deprotected polymers consist of hydrophobic POSS/OMe-LVF tripeptide chain ends and hydrophilic poly(L-glutamate) chains with side chain COO– moieties. Thus, these amphiphilic tripeptide–polymer conjugates may self-assemble to higher order structures in aqueous medium. First, we analyzed ^{1}H NMR spectra of **d1a** and **d2a** in D_2O (Fig. 1B and D). Resonance signals corresponding to the side chain glutamate residue are clearly observed but peaks originating from POSS/OMe-LVF tripeptide segments cannot be observed because water is a poor solvent for both the peptidic initiators but a good solvent for the appending glutamate residue at pH 8.0. This result clearly indicates higher-order structure formation by the benzyl deprotected peptide–polypeptide conjugates in water, most probably *via* suppression of the hydrophobic peptidic core which is surrounded by the hydrophilic carboxylic ion terminated glutamate residue.

Therefore, in the next stage self-assembling behaviour was investigated primarily by DLS measurements in aqueous medium at pH 8.0, from where average hydrodynamic diameters (D_h) of **d1a**, **d1b** and **d1c** were determined as 23 ± 3, 50 ± 7 and 120 ± 15 nm, respectively (Fig. 7). The D_h values for **d2a**, **d2b** and **d2c** were found to be 44 ± 5, 63 ± 9 and 189 ± 19 nm, respectively. In both the series, the D_h values considerably increase with increasing chain length of the hydrophilic segment. Interestingly, the average D_h values of **d1a–d1c** series were somewhat lower than the **d2a–d2c** series at comparable DP values. This could happen due to self-aggregation of the inorganic siloxane core in POSS moieties in the latter series.[47]

Self-assembling behaviors of benzyl deprotected polymers were further studied by FE-SEM (Fig. 8). Polymers **d1a**, **d1b** and **d1c** showed typical spherical nano-objects with average diameters of 60 ± 9, 71 ± 12 and 180 ± 20 nm, respectively. The average hydrodynamic diameter gradually increased with the

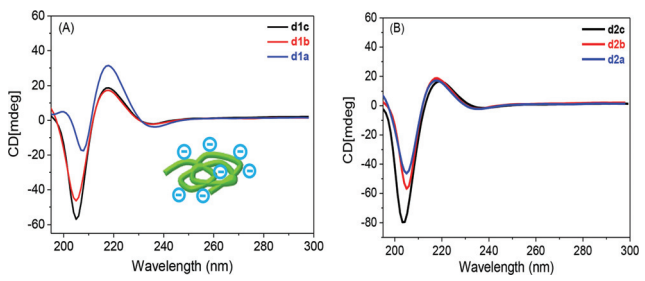

Fig. 6 CD spectra of deprotected (A) **d1a**, **d1b**, **d1c**, and (B) **d2a**, **d2b**, **d2c** in water at pH 8.0 at 20 °C.

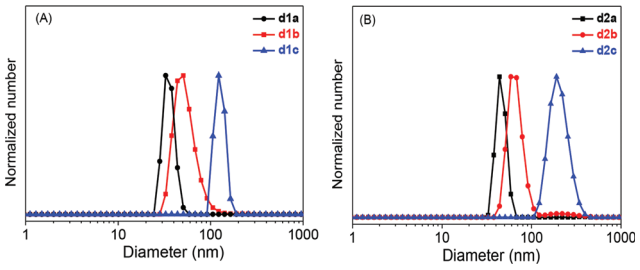

Fig. 7 Hydrodynamic diameter distribution for aqueous solutions (pH 8.0) of (A) **d1a**, **d1b**, **d1c**, and (B) **d2a**, **d2b**, **d2c**. Sample concentration: 0.5 mg mL^{-1}.

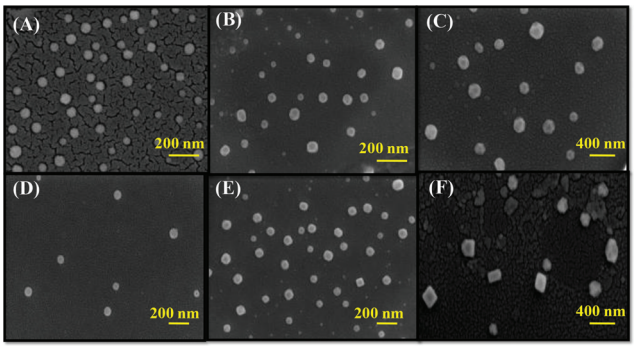

Fig. 8 FE-SEM images of (A) **d1a**, (B) **d1b**, (C) **d1c**, (D) **d2a**, (E) **d2b** and (F) **d2c**. Sample concentration: 0.1 mg mL^{-1}.

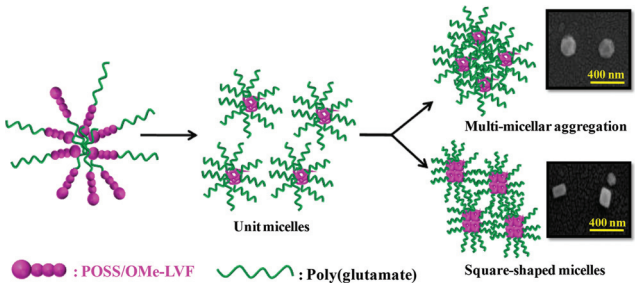

Fig. 9 Schematic representation of self-assembly by benzyl deprotected PBLG in aqueous medium at pH 8.0.

increasing length of the hydrophilic segment.[48] This kind of bigger spherical nano-objects can be attributed to multi-micellar aggregation driven by strong intermolecular hydrogen bonding interactions, which is a common phenomenon for multi-anion/cation charge containing amphiphilic polymers.[49,50] Interestingly, the spherical particles are well separated from each other due to the high charge density around the polymeric micelles, which helps them to avoid electrostatic repulsion by same charged species.[51] Similarly, **d2a** resulted in uniformly distributed spherical nano-objects with an average diameter of 78 ± 13 nm. In contrast, **d2b** gave both spherical and square morphologies with average diameters of 95 ± 15 nm, while **d2c** showed perfectly square type particles having diameter of 189 ± 22 nm. Polymers **d2a–d2c** are carrying POSS moiety at the chain end, which can influence the morphology due to the inherent self-aggregation property because of its inorganic siloxane hydrophobic core, which leads to formation of single layer crystals.[52] Nevertheless, the above studies confirmed that the hydrophobic POSS/OMe terminated tripeptide is located in the core and hydrophilic carboxylate ion containing poly(L-glutamate) chains are projected towards the corona of the micelles.

It is well documented in the literature that a single POSS molecule appended at the polymer chain can produce a wide spectrum of morphologies such as spherical, square-shaped, cylinders, ellipsoids, *etc.*[53,54] For example, a similar kind of square type self-assembled particles were formed by POSS end-functional poly(1-vinyl imidazole).[55] Transformation of spherical nano-objects to square shaped morphologies could be achieved from coalescence of spherical micelles with each other at a certain hydrophobic/hydrophilic ratio. Structural diversity governed by various benzyl deprotected polymers is represented pictorially in Fig. 9. Note that the apparent hydrodynamic diameters of self-assembled particles in aqueous medium obtained from DLS are somewhat bigger in comparison to the sizes obtained from FE-SEM analysis. This is because DLS measurements were carried out in aqueous phase, where the particles are in a hydrated state, while the FE-SEM was performed in the dry state.[56] Similarly, we investigated the self-assembly behaviour of **3a** (Fig. S25†). We observed D_h values of 35 ± 4 nm from DLS measurement (Fig. S25A†) for spherical particles (52 ± 7 nm from SEM analysis, Fig. S25B†), where butyl groups possibly induced some hydrophobicity in the system.

Conclusions

In conclusion, we have successfully synthesized organic/inorganic hybrid peptide-PBLG conjugates *via* grafting from ROP technique at room temperature with controllable molecular weights and narrow $Đ$ values. FT-IR spectroscopy showed a characteristic peak at 1652 cm^{-1} (amide-I) for main chain PBLG, an indicative band of α-helix conformation. The PXRD diffraction peak at $2\theta = 6.30°$ represents the intermolecular distance between the two adjacent peptide chains within one lamella having 2D hexagonal packing of cylinders comprised of 18/5 α-helices. Solution-state CD study with OMe/POSS-peptide-PBLG conjugates displayed one negative signal at 222 nm due to the n–π* electronic transition, which is signature band of the α-helical secondary structure. FE-SEM and AFM images of these conjugates showed entangled helical nano-fibres due to hierarchical self-organization governed by the chiral PBLG segments. Clearly, incorporation of the sequence registered OMe/POSS-LVF peptide at the chain end of PBLG segment did not disturb the α-helical secondary conformation of PBLG in either the solid or solution state. Benzyl group deprotection from these conjugates produced a wide spectrum of morphological transitions, from spherical to square-shaped particles. Therefore, π–π aromatic interactions between side chain phenyl groups in PBLG induced stable helical conformations in OMe/POSS-LVF-PBLG conjugates. In the benzyl deprotected polymers, the hydrophobic POSS/OMe terminated tripeptide is located in the core and hydrophilic carboxylate ion containing poly(L-glutamate) chains are projected towards the corona of the micelles in aqueous medium. Here, a judicious balance of hydrophobic/hydrophilic segments as well as the content of crystalline POSS moiety is important to get a square-type morphology.

Acknowledgements

This work was supported by the Defence Research and Development Organisation (DRDO), India [Project no.

ERIP/ER/1001116/M/01]. We thank Dr Suhrit Ghosh and Mr Prithankar Pramanik from Indian Association for the Cultivation of Science (IACS), Kolkata for allowing us to use their GPC facility. U. Haldar and I. Mukherjee thank Council of Scientific and Industrial Research (CSIR), Government of India, for their fellowships. A. Pan is grateful to Department of Science and Technology (DST), Government of India for INSPIRE scholarship.

Notes and references

1 Y. Bae, S. Fukushima, A. Harada and K. Kataoka, *Angew. Chem., Int. Ed.*, 2003, **42**, 4640–4643.
2 H. R. Kricheldorf, *Angew. Chem., Int. Ed.*, 2006, **45**, 5752–5784.
3 R. Duncan, *Nat. Rev. Drug Discovery*, 2003, **2**, 347–360.
4 E. S. Place, N. D. Evans and M. M. Stevens, *Nat. Mater.*, 2009, **8**, 457–470.
5 A. M. Kloxin, A. M. Kasko, C. N. Salinas and K. S. Anseth, *Science*, 2009, **324**, 59–63.
6 H. A. Klok and S. Lecommandoux, *Adv. Mater.*, 2001, **13**, 1217–1229.
7 C. Robinson and J. C. Ward, *Nature*, 1957, **180**, 1183–1184.
8 Y. C. Lin and S. W. Kuo, *Polym. Chem.*, 2012, **3**, 162–171.
9 Y. C. Lin and S. W. Kuo, *Polym. Chem.*, 2012, **3**, 882–891.
10 S. W. Kuo, H. F. Lee, W. J. Huang, K. U. Jeong and F. C. Chang, *Macromolecules*, 2009, **42**, 1619–1626.
11 J. Cheng and T. J. Deming, *Top. Curr. Chem.*, 2012, **310**, 1–26.
12 M. Morel and J. Puiggal, *Polymers*, 2013, **5**, 188–224.
13 T. J. Deming, *Prog. Polym. Sci.*, 2007, **32**, 858–875.
14 H. R. Marsden, J. W. Handgraaf, F. Nudelman, N. A. J. M. Sommerdijk and A. Kros, *J. Am. Chem. Soc.*, 2010, **132**, 2370–2377.
15 H. Enomoto, B. Nottelet, S. A. Halifa, C. Enjalbal, M. Dupre, J. Tailhades, J. Coudane, G. Subra, J. Martinez and M. Amblard, *Chem. Commun.*, 2013, **49**, 409–411.
16 J. Y. Shu, B. Panganiban and T. Xu, *Annu. Rev. Phys. Chem.*, 2013, **64**, 631–657.
17 S. Dehn, R. Chapman, K. A. Jolliffe and S. Perrier, *Polym. Rev.*, 2011, **51**, 214–234.
18 H. G. Borner, *Prog. Polym. Sci.*, 2009, **34**, 811–851.
19 S. Basak, V. D. Punetha, G. Bisht, S. S. Bisht, N. G. Sahoo and J. W. Cho, *Polym. Rev.*, 2015, **55**, 163–198.
20 B. Urbanc, L. Cruz, S. Yun, S. V. Buldyrev, G. Bitan, D. B. Teplow and H. E. Stanley, *Proc. Natl. Acad. Sci. U. S. A.*, 2004, **101**, 17345–17350.
21 H. Skaat, R. Chen, I. Grinberg and S. Margel, *Biomacromolecules*, 2012, **13**, 2662–2670.
22 E. Sarubbi, P. F. Seneci, M. R. Angelastro, N. P. Peet, M. Denaro and K. Islam, *FEBS Lett.*, 1993, **319**, 253–256.
23 R. L. Johnson, *J. Med. Chem.*, 1982, **25**, 605–610.
24 S. W. Kuo, H. F. Lee, W. J. Huang, K. U. Jeong and F. C. Chang, *Macromolecules*, 2009, **42**, 1619–1626.
25 D. B. Cordes, P. D. Lickiss and F. Rataboul, *Chem. Rev.*, 2010, **110**, 2081–2173.
26 Y. C. Lin and S. W. Kuo, *J. Polym. Sci., Part A: Polym. Chem.*, 2011, **49**, 2127–2137.
27 S. W. Kuo and H. T. Tasai, *Polymer*, 2010, **51**, 5695–5704.
28 B. S. Furniss, A. J. Hannaford, P. W. G. Smith and A. R. Tatchell, *Vogel's Textbook of Practical Organic Chemistry*, Longman Scientific & Technical, co-published in the USA with John Wiley & Sons, Inc, New York, 1989.
29 S. Kumar, V. Bheemireddy and P. De, *Macromol. Biosci.*, 2015, **15**, 1447–1456.
30 M. R. Molla, P. Prasad and S. Thayumanavan, *J. Am. Chem. Soc.*, 2015, **137**, 7286–7289.
31 C. D. Vacogne, S. M. Brosnan, A. Masic and H. Schlaad, *Polym. Chem.*, 2015, **6**, 5040–5062.
32 N. Hadjichristidis, H. Iatrou, M. Pitsikalis and G. Sakellariou, *Chem. Rev.*, 2009, **109**, 5528–5578.
33 U. Haldar, M. Nandi, B. Ruidas and P. De, *Eur. Polym. J.*, 2015, **67**, 274–283.
34 S. Motala-Timol, D. Jhurry, J. W. Zhou, A. Bhaw-Luximon, G. Mohun and H. Ritter, *Macromolecules*, 2008, **41**, 5571–5576.
35 D. Müller and H. R. Kricheldorf, *Polym. Bull.*, 1981, **6**, 101–108.
36 P. Papadopoulos, G. Floudas, H. A. Klok, I. Schnell and T. Pakula, *Biomacromolecules*, 2004, **5**, 81–91.
37 C. H. Cai, J. P. Lin, T. Chen and X. H. Tian, *Langmuir*, 2010, **26**, 2791–2797.
38 J. Wang, H. Lu, R. Kamat, S. V. Pingali, V. S. Urban, J. Cheng and Y. Lin, *J. Am. Chem. Soc.*, 2011, **133**, 12906–12909.
39 W. Li, X. Q. Zhang, J. Wang, X. Qiao, K. Liu and A. F. Zhang, *J. Polym. Sci., Part A: Polym. Chem.*, 2012, **50**, 4063–4072.
40 H. Tang, Y. Li, S. H. Lahasky, S. S. Sheiko and D. Zhang, *Macromolecules*, 2011, **44**, 1491–1499.
41 S. Zhai, X. Song, C. Feng, X. Jiang, Y. Li, G. Lu and X. Huang, *Polym. Chem.*, 2013, **4**, 4134–4144.
42 C. Cai, J. Lin, X. Zhu, S. Gong, X. S. Wang and L. Wang, *Macromolecules*, 2016, **49**, 15–22.
43 L. Hua, J. Wang, B. Yugang, J. W. Lang, L. Shiyong, Y. Lin and J. Cheng, *Nat. Commun.*, 2011, **2**, 1–9.
44 K. S. Krannig and H. Schlaad, *J. Am. Chem. Soc.*, 2012, **134**, 18542–18545.
45 V. Abetz and P. F. W. Simon, *Adv. Polym. Sci.*, 2005, **189**, 125–212.
46 W. A. Zhang, B. Fang, A. Walther and A. H. E. Müller, *Macromolecules*, 2009, **42**, 2563–2569.
47 W. A. Zhang, J. Yuan, S. Weiss, X. Ye, C. Li and A. H. E. Müller, *Macromolecules*, 2011, **44**, 744–750.
48 W. A. Zhang, L. Liu, X. D. Zhuang, X. H. Li, J. R. Baiand and Y. Chen, *J. Polym. Sci., Part A: Polym. Chem.*, 2008, **46**, 7049–7061.
49 A. Saha, T. K. Paira, M. Biswas, S. Jana, S. Banerjee and T. K. Mandal, *J. Polym. Sci., Part A: Polym. Chem.*, 2015, **53**, 2313–2319.
50 Y. Tang, L. Liu, J. Wu and J. Duan, *J. Colloid Interface Sci.*, 2013, **397**, 24–31.

51 K. Bauri, S. G. Roy, S. Pant and P. De, *Langmuir*, 2013, **29**, 2764–2774.
52 U. Haldar, S. G. Roy and P. De, *Polymer*, 2016, **97**, 113–121.
53 J. Cai, C. Lv and A. Watanabe, *ACS Appl. Mater. Interfaces*, 2015, **7**, 18697–18706.
54 W. Zhang and A. H. E. Müller, *Prog. Polym. Sci.*, 2013, **38**, 1121–1162.
55 M. Dule, M. Biswas, T. K. Paira and T. K. Mandal, *Polymer*, 2015, **77**, 32–41.
56 S. G. Roy and P. De, *Polym. Chem.*, 2014, **5**, 6365–6378.